Eur. Phys. J. B **49**, 415–420 (2006)
DOI: 10.1140/epjb/e2006-00093-1

THE EUROPEAN PHYSICAL JOURNAL B

Electronic structure of ZnO wurtzite quantum wires

J.B. Xia and X.W. Zhang[a]

Chinese Center of Advanced Science and Technology (World Laboratory), Beijing 100080, R.P. China,
and
Institute of Semiconductors, Chinese Academy of Sciences, Beijing 100083, R.P. China

Received 1st December 2005 / Received in final form 24 January 2006
Published online 31 March 2006 –

Abstract. The electronic structure and optical properties of ZnO wurtzite quantum wires with radius $R \geq 3$ nm are studied in the framework of six-band effective-mass envelope function theory. The hole effective-mass parameters of ZnO wurtzite material are calculated by the empirical pseudopotential method. It is found that the electron states are either two-fold or four-fold degenerate. There is a dark exciton effect when the radius R of the ZnO quantum wires is in the range of $[3, 19.1]$ nm (dark range in our model). The dark ranges of other wurtzite semiconductor quantum wires are calculated for comparison. The dark range becomes smaller when the $|\Delta_{so}|$ is larger, which also happens in the quantum-dot systems. The linear polarization factor of ZnO quantum wires is larger when the temperature is higher.

PACS. 73.21.Hb Quantum wires – 78.67.Lt Quantum wires

1 Introduction

Low dimensional systems such as semiconductor quantum dots and quantum wires have fascinating and technologically useful optical and electric properties. Studies on these systems advance our knowledge on low dimensional physics and chemistry. Semiconductor quantum wires exhibit novel electric and optical properties owing to their unique structural one-dimensionality and possible quantum confinement effects in two dimensions. Quantum wires have been evaluated for potential applications as laser [1–4], light-emitting diodes [5], and photodetectors [6–8].

Nowadays the methods to synthesize quantum wires have been improved. ZnO wurtzite quantum wires in a large range of radius are synthesized by different methods [9,11–17] and whose shape can also be controlled [11]. Their temperature dependent PL spectra [13,18], photomodulated transmittance spectroscopy [19], size-dependent surface luminescence [20] and Raman spectrum [9] are measured. Recently much attention has been paid to the linear polarized optical property of quantum wires. Linear polarized emissions from quantum wires are observed and explained by dielectric effect [22], or quantum confinement effect [23,24]. Actually, ZnO wurtzite single crystal bulk material [25] also have linear polarized emissions.

[a] e-mail: zhxw99@semi.ac.cn

The electronic structures of nanowires with zinc-blende structure have been studied in the framework of six-band effective-mass approximation [26]. In this paper, we expand the former model to nanowires of the wurtzite structure, and apply the new model to investigate the electronic structure and optical properties of wurtzite quantum wires. The remainder of this paper is organized as follows. In Section 2 we give the form of the Hamiltonian. Our numerical results and discussions are given in Section 3. Finally, we draw a brief conclusion in Section 4.

2 Model and calculation

There were few energy band calculations for hexagonal ZnO, for example the empirical pseudopotential calculation [27] and the self-consistent pseudopotential calculation [28]. We represent the form factor of the atomic pseudopotential with a continuous function of the wave vector q by the Cohen's formula [29],

$$V(q) = \frac{v_1\left(q^2 - v_2\right)}{\exp\left[v_3\left(q^2 - v_4\right)\right] + 1}, \tag{1}$$

where the unit of q is au, and the unit of $V(q)$ is Ry. There are 4 parameters $v_1 - v_4$ for the Zn atom, and 4 parameters for the O atom. By comparing the calculated energy bands with previous theoretical results [27,28] and experiments, we determined the 8 pseudopotential parameters

$$H_{h0} = -\frac{1}{2m_0}\begin{vmatrix} Lp_x^2 + Mp_y^2 + Np_z^2 & Rp_xp_y & Qp_xp_z \\ Rp_xp_y & Lp_y^2 + Mp_x^2 + Np_z^2 & Qp_yp_z \\ Qp_xp_z & Qp_yp_z & S\left(p_x^2 + p_y^2\right) + Tp_z^2 + 2m_0\Delta_c \end{vmatrix}, \quad (2)$$

Table 1. Atom pseudopotential parameters.

	v_1	v_2	v_3	v_4		v_1	v_2	v_3	v_4
Zn	0.11003	1.79208	0.80055	4.25370	O	0.19597	4.90951	1.24475	3.60095

Table 2. ZnO effective-mass parameters of hole.

L	M	N	R	S	T	Q
5.62	0.28	0.435	5.34	0.416	6.22	3.22

for ZnO, which are listed in Table 1. The hole effective-mass Hamiltonian for wurtzite semiconductors in the case of zero spin-orbital coupling is given by [30]

see equation (2) above

where the valence band basis functions are X-like, Y-like (Γ_6) and Z-like (Γ_1) functions, respectively, L, M, $\cdots$, S, T are effective-mass parameters. Δ_c is the crystal field splitting energy. By comparing the valence bands near the top calculated by the effective-mass Hamiltonian (2) and by the empirical pseudopotential method, we determined uniquely the effective-mass parameters in Hamiltonian (2), as shown in Table 2 for ZnO.

Hereafter we assume that the wire is along the z axis of the crystal structure, and the cylinder has a sharp boundary, so that the wave functions at the boundary are zero. The sharp boundary is only suitable for thicker wires, so we only calculate the electronic structure and optical properties of wurtzite quantum wires with radius $R \geq 3$ nm. In order to calculate in the cylindrical coordinate, we transform the hole Hamiltonian (2) from the basis functions X, Y, and Z to the $1\sqrt{2}\,(X+iY)$, $1/\sqrt{2}\,(X-iY)$, and Z,

$$H_{h0} = -\frac{1}{2m_0}\begin{vmatrix} P_1 & F & G \\ F^* & P_1 & G^* \\ G^* & G & P_3 \end{vmatrix}, \quad (3)$$

where

$$\begin{aligned} P_1 &= \frac{L+M}{2}p_-p_+ + Np_z^2, \\ P_3 &= Sp_-p_+ + Tp_z^2 + 2m_0\Delta_c, \\ F &= \frac{L-M-R}{4}p_+^2 + \frac{L-M+R}{4}p_-^2, \\ G &= \frac{1}{\sqrt{2}}Qp_-p_z, \\ p_\pm &= p_x \pm ip_y. \end{aligned} \quad (4)$$

The spin-orbital coupling (SOC) Hamiltonian is written as [26],

$$H_{so} = -\begin{vmatrix} 0 & 0 & 0 & 0 & 0 & 0 \\ 0 & 2\lambda & 0 & 0 & 0 & -\sqrt{2}\lambda \\ 0 & 0 & \lambda & \sqrt{2}\lambda & 0 & 0 \\ 0 & 0 & \sqrt{2}\lambda & 2\lambda & 0 & 0 \\ 0 & 0 & 0 & 0 & 0 & 0 \\ 0 & -\sqrt{2}\lambda & 0 & 0 & 0 & \lambda \end{vmatrix}, \quad (5)$$

where

$$\lambda = \frac{\hbar^2}{4m_0^2c^2}\left\langle X\left|\frac{\partial V}{\partial x}\frac{\partial}{\partial y}\right|Y\right\rangle = \frac{\Delta_{so}}{3}. \quad (6)$$

Here, we take the basis functions as $1/\sqrt{2}\,(X+iY)\uparrow$, $1/\sqrt{2}\,(X-iY)\uparrow$, $Z\uparrow$, $1/\sqrt{2}\,(X+iY)\downarrow$, $1/\sqrt{2}\,(X-iY)\downarrow$ and $Z\downarrow$. The eigenvalues of the SOC Hamiltonian H_{so} are 3λ and 0, the latter is taken as the energy origin. We make the cylindrical symmetry approximation for the valence bands, i.e. assume that the coefficient of the p_+^2 term in F of equation (4) is zero, $L-M-R=0$, which is verified from Table 2.

In the cylindrical symmetry approximation, we expand the wave function of the hole state in Bessel functions,

$$\phi_{J,k} = \sum_n \begin{pmatrix} b_{L-1,k,n,\uparrow}A_{L-1,n}J_{L-1}\left(k_n^{L-1}r\right)e^{i(L-1)\theta} \\ c_{L+1,k,n,\uparrow}A_{L+1,n}J_{L+1}\left(k_n^{L+1}r\right)e^{i(L+1)\theta} \\ d_{L,k,n,\uparrow}A_{L,n}J_L\left(k_n^Lr\right)e^{iL\theta} \\ b_{L,k,n,\downarrow}A_{L,n}J_L\left(k_n^Lr\right)e^{iL\theta} \\ c_{L+2,k,n,\downarrow}A_{L+2,n}J_{L+2}\left(k_n^{L+2}r\right)e^{i(L+2)\theta} \\ d_{L+1,k,n,\downarrow}A_{L+1,n}J_{L+1}\left(k_n^{L+1}r\right)e^{i(L+1)\theta} \end{pmatrix} e^{ikz}, \quad (7)$$

where $J = L + 1/2$ is the total azimuthal angular momentum, and $A_{L,n}$ is the normalization constant,

$$A_{L,n} = \frac{1}{\sqrt{\pi}RJ_{L+1}\left(\alpha_n^L\right)}, \quad (8)$$

$\alpha_n^L = k_n^L R$ is the nth zero of the Bessel function $J_L(x)$, R is the radius of the cylinder, and k is the wave vector along the z direction. In the cylindrical symmetry, the system has the conserved quantum number k and J, the total azimuthal angular momentum. Therefore the summation in equation (7) is only over n. In calculating the matrix elements of the Hamiltonian equation (3) we can use the property of the operators $p_\pm$,

$$p_\pm J_L\left(k_n^Lr\right)e^{iL\theta} = \mp\frac{\hbar}{i}k_n^LJ_{L\pm1}\left(k_n^Lr\right)e^{i(L\pm1)\theta}. \quad (9)$$

The electron Hamiltonian is

$$H_{e0} = \frac{1}{2m_x^*} p_- p_+ + \frac{1}{2m_z^*} p_z^2 + E_g', \tag{10}$$

where $E_g' = E_g$ when $\Delta_{so} > 0$ and $E_g' = E_g - \Delta_{so}$ when $\Delta_{so} < 0$. We take the basis functions as $S\uparrow$ and $S\downarrow$, S is the Bloch state of conduction-band bottom. The wave function of the electron state is expanded in Bessel functions,

$$\phi_{J,k}^e = \sum_n \begin{pmatrix} e_{L,k,n,\uparrow} A_{L,n} J_L\left(k_n^L r\right) e^{iL\theta} \\ e_{L+1,k,n,\downarrow} A_{L+1,n} J_{L+1}\left(k_n^{L+1} r\right) e^{i(L+1)\theta} \end{pmatrix} e^{ikz}. \tag{11}$$

We also calculate the linear polarization factor of the wires, and assume that the light wave propagates along the y direction. We do not include the electron-hole interaction in our calculations as our approach is a single-particle approach. The linear polarization factor is affected by the quantum confinement effect and the dielectric effect. At first we taking into account only the quantum confinement effect. As $\langle S|P_t|X\rangle = \langle S|P_t|Y\rangle = \langle S|P_t|Z\rangle$ (S, X, Y, Z are the Bloch states and P_t is the optical transition operator), the intensities of the optical transitions are proportional to the overlap of the envelop functions of electron and hole states. That is to say, with the optical transition between a given electron state and a given hole state, the intensities of z and x polarized transitions are proportional to

$$I_z = \left\{ \sum_{L,k,n,s} d_{L,k,n,s} e_{L,k,n,s} \right\}^2, \tag{12}$$

$$I_x = \left\{ \sum_{L,k,n,s} (b_{L,k,n,s} e_{L,k,n,s} + c_{L,k,n,s} e_{L,k,n,s})/\sqrt{2} \right\}^2, \tag{13}$$

where s denotes spin-up $\uparrow$ or spin-down $\downarrow$, $b_{L,k,n,s}$, $c_{L,k,n,s}$, $d_{L,k,n,s}$ and $e_{L,k,n,s}$ are given in equations (7) and (11), respectively.

For the wires, the dielectric effect vanishes in the z direction, but remains in the perpendicular directions. So the z polarized transition is not affected, but the x polarized transition is decreased [22], that is to say

$$I_z' = I_z, \tag{14a}$$

$$I_x' = \frac{I_x}{W}, \tag{14b}$$

$$W = \frac{(\varepsilon_{\mathrm{ZnO}} + \varepsilon_0)^2 + 2\varepsilon_0^2}{6\varepsilon_0^2} > 1, \tag{14c}$$

where $\varepsilon_{\mathrm{ZnO}}$ and ε_0 are the dielectric constants in and outside the wire. Then the linear polarization factor is calculated approximately by

$$P = (I_z' - I_x')/(I_z' + I_x') = (I_z W - I_x)/(I_z W + I_x), \tag{15}$$

where I_z and I_x are given by equations (12) and (13). Considering the temperature effect, we multiply the Boltzmann distribution factor to each state, and sum up all contributions to the intensities.

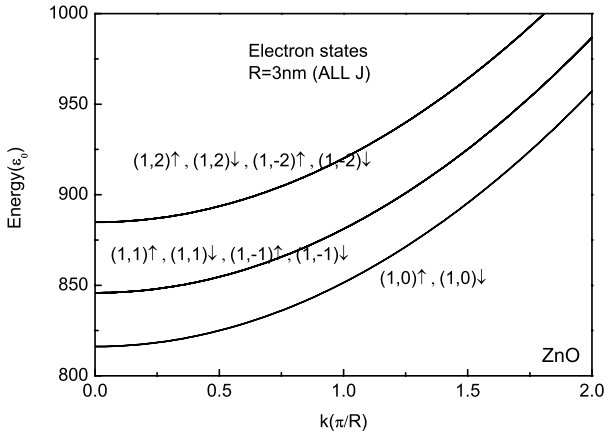

Fig. 1. Electron states (all J) of ZnO quantum wire with radius of $R = 3$ nm as functions of k.

3 Results and discussions

We calculated the electronic structure and optical properties of ZnO wurtzite quantum wires with radius $R \geq 3$ nm. Except the effective-mass parameters in Hamiltonian (2) shown in Table 2, other parameters used in this paper are taken as: the electron effective masses perpendicular to and along the c axis, $m_x^* = 0.3m_0$ and $m_z^* = 0.28m_0$, respectively. The dielectric constant $\varepsilon_{\mathrm{ZnO}} = 8.331$ [31], the band gap $E_g = 3.37$ eV [9,10], the crystal field splitting energy $\Delta_c = 0.03942$ eV and the spin-orbit splitting energy $\Delta_{so} = -0.00352$ eV [31,35]. The unit of energy is

$$\varepsilon_0 = \frac{1}{2m_0} \left(\frac{\hbar}{R}\right)^2. \tag{16}$$

3.1 Electronic structure

The electron states (all J) of ZnO quantum wires with radius of $R = 3$ nm as functions of k are shown in Figure 1. The symbol of each energy level represents the main components of it's wave function. For example, $(1,0)\uparrow$ means that the state consists mainly of the $n = 1$, $L = 0$ state of the effective-mass envelope function multiplied with the S Bloch state of the conduction-band bottom and the spin-up state. We see that the electron states are degenerate. For $L = 0$, they are two-fold degenerate with spin-up and spin-down states. For $L \neq 0$, they are four-fold degenerate with $\pm L$ and spin-up, spin-down states. The energy levels increase with increasing k as quadratic terms of k, due to the quadratic terms of p_z in equation (4). The hole states of ZnO quantum wires with radius of $R = 3$ nm and $J = 1/2$ as functions of k are shown in Figure 2. The hole states of ZnO quantum wires with radius of $R = 3$ nm and $J = 3/2$ as functions of k are shown in Figure 3. The symbol of each energy level represents the main components of it's wave function. For example, $(1,0)X^+\uparrow$ means that the state consists mainly of the $n = 1$, $L = 0$ state of the effective-mass envelope function multiplied with the $1/\sqrt{2}\,(X + iY)$ Bloch state of the valence-band top and

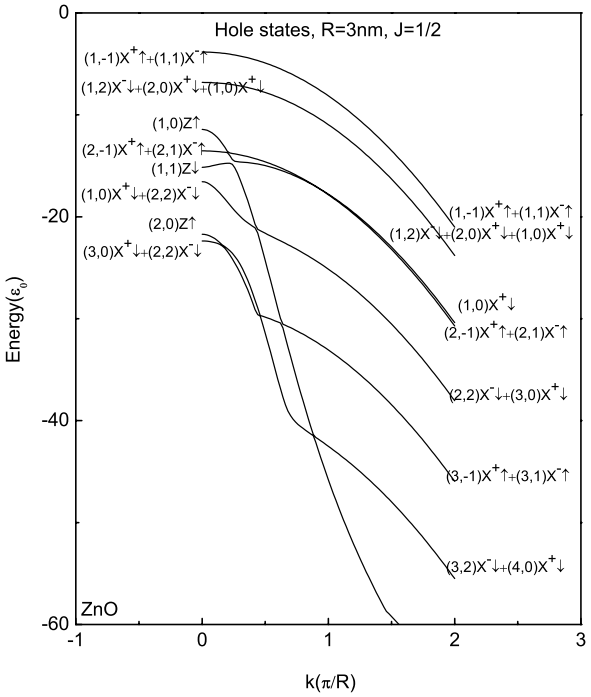

Fig. 2. Hole states of ZnO quantum wire with radius of $R = 3$ nm and $J = 1/2$ as functions of k.

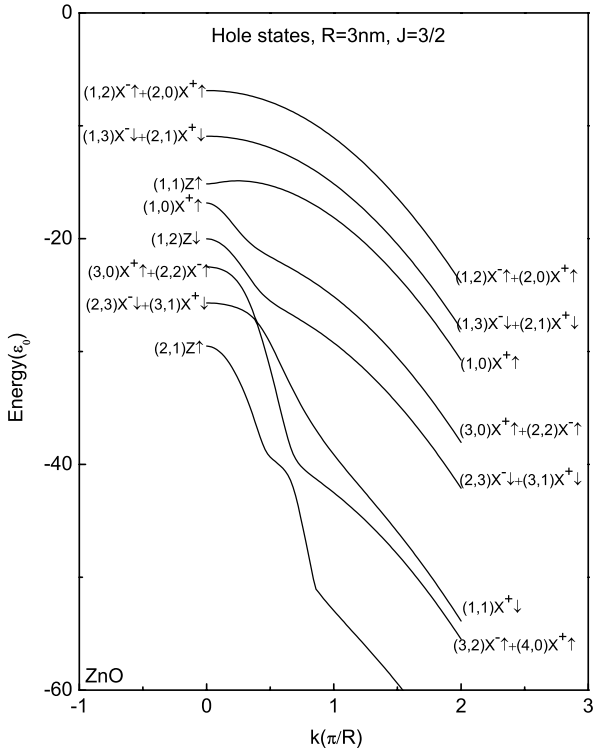

Fig. 3. Hole states of ZnO quantum wire with radius of $R = 3$ nm and $J = 3/2$ as functions of k.

the spin-up state. We see that most of the energy levels decrease as k increases, few of the energy levels increase at first, due to the coupling of the states, then decrease as k increases. The levels of the states with Z Bloch state decrease more quickly than the levels of the states with $1/\sqrt{2}\,(X + iY)$ and $1/\sqrt{2}\,(X - iY)$ Bloch states. This is because that the coefficients of the p_z^2 terms in equation (4) of the two kinds of basic states Z and X, Y are different, which are T and N, respectively, and T is much greater than N as shown in Table 2. This is similar to the light and heavy hole effect. It is noticed that the hole states with $\pm J$ are degenerate, so the hole states in Figures 2 and 3 are all two-fold degenerate. The wave functions of the $-J$ hole states are those of the $+J$ states denoted in Figures 2 and 3 with the reversed spin states. The degeneracy of states with $+J$ and $-J$ is known as Kramers degeneracy.

The electron states (all J) of ZnO quantum wires at $k = 0$ as functions of R are shown in Figure 4a. We see that when R is larger than 20 nm, all the levels come down to a same value, i.e. E_g' given in equation (10), that means that the quantum confinement effect vanishes. The band gap of ZnO quantum wires as a function of R is shown in Figure 4b. We define the band gap of ZnO quantum wires as the separation between the ground electron and hole subband states at $k = 0$. We see that it is much larger than $E_g = 3.37$ eV when R is small, due to quantum confinement effect, and is nearly 3.37 eV when R is larger than 20 nm.

The hole states ($J = 1/2, 3/2$) of ZnO quantum wires at $k = 0$ as functions of R are shown in Figure 4c. Because the highest energy level of valence-band decrease

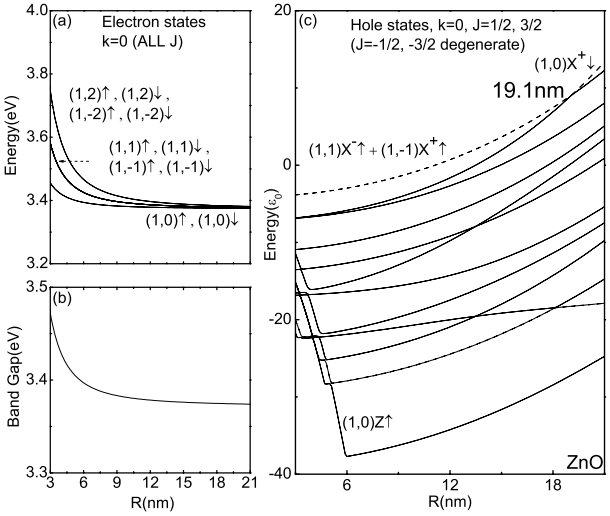

Fig. 4. (a) Electron states (all J) of ZnO quantum wires with $k = 0$ as functions of R. (b) Band gap of ZnO quantum wires as a function of R. (c) Hole states ($J = 1/2, 3/2$) of ZnO quantum wires with $k = 0$ as functions of R.

with increasing k (see Fig. 2), the highest state at $k = 0$ in Figure 4c is the ground state of valence-band. The energy is in the unit of ε_0. We see that the levels of the states which have dominating Z Bloch state components (e.g. $(1,0)Z\uparrow$) decrease very quickly as R increases, due to $\Delta_c > 0$. The levels of the states which have dominating spin-orbit split-off state components (e.g. $(1,0)X^+\downarrow$) increase as R increases, due to $\Delta_{so} < 0$. The levels

of the states which have dominating spin-orbit split-off state components and also dominating heavy-hole components (e.g. $(1,1)X^- \uparrow +(1,-1)X^+ \uparrow$) increase slowly as R increases. It is noticed that the wave function of the ground state changes as R increases. When R is larger than 19.1 nm, the highest state is $(1,0)X^+ \downarrow$. When R is in the range of $[3, 19.1]$ nm, the highest state is $(1,1)X^- \uparrow +(1,-1)X^+ \uparrow$, a state with $L = \pm 1$, which is different from $L = 0$ of the lowest state of conduction-band. At low temperature, the electron and hole distribute in the lowest state of conduction-band and the highest state of valence-band, respectively. So when R is in the range of $[3, 19.1]$ nm, which we named as the dark range (restricted by the range of radius which can be calculated in our model), the electron and hole can not be recombined directly, that means that there is a dark exciton effect. The crossing of the levels $(1,0)X^+ \downarrow$ and $(1,1)X^- \uparrow +(1,-1)X^+ \uparrow$ is because that the former increases more quickly than the latter as R increases. When the $|\Delta_{so}|$ is increased, the highest two energy levels all increase more quickly, and the crossing point moves to smaller radius.

The dark exciton effect is due to the wurtzite crystal structure and the quantum confinement effect, which leads to a new order of the hole energy levels different from the order in bulk material. We also calculate the dark ranges of CdS, CdSe wurtzite quantum wires. The effective-mass parameters are cited from Xia et al. [33]. The splitting energies are $\Delta_{so} = 70$ meV, $\Delta_c = 24$ meV for CdS [34], and $\Delta_{so} = 418$ meV, $\Delta_c = 40$ meV for CdSe [35]. The calculated dark ranges in our model of CdS, CdSe wurtzite quantum wires are $[3, 6.2]$ nm, $[3, 4.0]$ nm, respectively, as shown in Figure 5. We see that all the levels decrease as R increases, because $\Delta_c > 0$ and $\Delta_{so} > 0$. As R increases, the hole ground state changes from $(1,-1)X^+ \uparrow +(1,1)X^- \uparrow$ to $(1,0)X^+ \uparrow$ which is a heavy-hole state, as shown in Figure 5. We see that the dark range becomes smaller, from CdS to CdSe, due to the similar reason to the ZnO case as the $|\Delta_{so}|$ of CdS is smaller than that of CdSe. Xia et al. [33,34] calculated out that CdS quantum dots with radius smaller 6.9 nm which was named as the critical radius, and CdSe quantum dots with radius of $R < 3$ nm have dark exciton effect. The critical radius of CdS quantum dots is larger than that of CdSe quantum dots, due to the similar reason to the wire case (see Fig. 5) as the $|\Delta_{so}|$ of CdS is smaller than that of CdSe.

So there is a dark exciton effect in the wurtzite quantum wires and dots, and the dark range becomes smaller with the $|\Delta_{so}|$ increasing, i.e. becomes larger with the $|\Delta_{so}|$ decreasing.

3.2 Linear polarization

We calculate the linear polarization factor of the wire, taking into account the quantum confinement effect and the dielectric effect. The dielectric constants are $\varepsilon_{\mathrm{ZnO}} = 8.331$ [31] in the wire, and $\varepsilon_0 = 1$ in the vacuum, then $W = 14.8446$ (see Eq. (14)). The linear polarization factors of ZnO quantum wires as functions of R are shown in Figure 6a. We see that the linear polarization factor is dependent on the radius and the temperature, and decreases as R increases. It is noticed that at higher temperature, the linear polarization factor is larger, which is opposite to the CdSe ellipsoid case [24]. Actually, the virtual linear polarization factors taking into account only the quantum confinement effect are mostly negative, as shown in Figure 6b, and the absolute value of the linear polarization factor at higher temperature is smaller. The dielectric effect corrects this virtual result to the real result by the factor W in equation (15), and the relative position of the polarization factors at different temperature does not change.

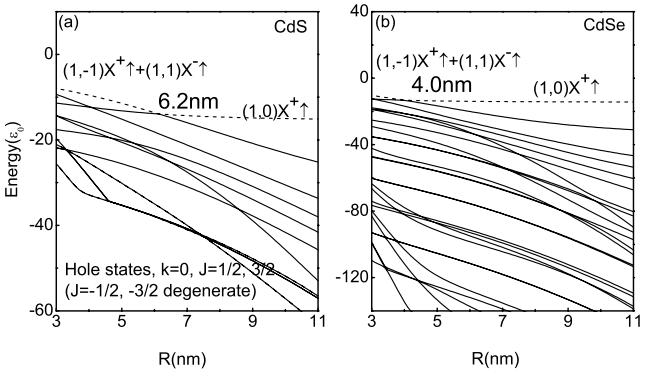

Fig. 5. Hole states ($J = 1/2, 3/2$) of CdS and CdSe quantum wires with $k = 0$ as functions of R. (a) CdS; (b) CdSe.

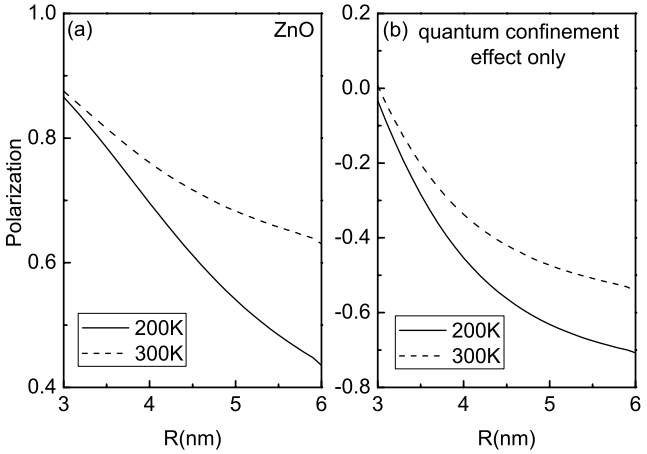

Fig. 6. (a) Linear polarization factors of ZnO quantum wires as functions of R. (b) Virtual linear polarization factors of ZnO quantum wires taking into account only the quantum confinement effect as functions of R.

4 Conclusion

The electronic structure and optical properties of ZnO wurtzite quantum wires with radius $R \geq 3$ nm are studied in the framework of six-band effective-mass envelope function theory. The hole effective-mass parameters of ZnO wurtzite material are calculated by the empirical pseudopotential method. It is found that the electron states

are either two-fold or four-fold degenerate. There is a dark exciton effect in the wurtzite quantum wires and dots, due to the wurtzite crystal structure and the quantum confinement effect, which leads to a new order of the hole energy levels different from the order in bulk material. The dark ranges in our model of the ZnO, CdS and CdSe quantum wires are $[3, 19.1]$ nm, $[3, 6.2]$ nm and $[3, 4]$ nm, respectively. The dark range becomes smaller when the $|\Delta_{so}|$ is larger, which also happens in the quantum-dot systems. The linear polarization factor of ZnO quantum wires is larger when the temperature is higher.

This work is supported by the National Natural Science Foundation of China No. 90301007, 60521001 and the special funds for Major State Basic Research Project No. G001CB3095 of China.

References

1. Zhiren Qiu, K.S. Wong, Mingmei Wu, Wenjiao Lin, Huifang Xu, Appl. Phys. Lett. **84**, 2739 (2004)
2. Li Cao, Bingsuo Zou, Chaorong Li, Zebo Zhang, Sishen Xie, Guozhen Yang, Europhys. Lett. **68**, 740 (2004)
3. Xiangfeng Duan, Yu Huang, Ritesh Agarwal, C.M. Lieber, Nature **421**, 241 (2003)
4. P. Yang, H. Yan, S. Mao, R. Russo, J. Johnson, R. Saykally, N. Morris, J. Pham, R. He, H.-J. Choi, Adv. Funct. Mater. **12**, 323 (2002)
5. C.H. Liu, J.A. Zapien, Y. Yao, X.M. Meng, C.S. Lee, S.S. Fan, Y. Lifshitz, S.T. Lee, Adv. Mater. (Weinheim, Ger.) **15**, 838 (2003)
6. Biswajit Das, Pavan Singaraju, Infrared Physics and Technology **46**, 209 (2005)
7. H. Kind, H. Yan, B. Messer, M. Law, P. Yang, Adv. Mater. (Weinheim, Ger.) **14**, 158 (2002)
8. K. Keem, H. Kim, G.-T. Kim, J.S. Lee, B. Min, K. Cho, M.-Y. Sung, S. Kim, Appl. Phys. Lett. **84**, 4376 (2004)
9. Xuan Wang, Qingwen Li, Zhibo Liu, Jin Zhang, Zhongfan Liu, Rongming Wang, Appl. Phys. Lett. **84**, 4941 (2004)
10. J. Wrzesinski, D. Frohlich, Phys. Rev. B **56**, 13087 (1997)
11. Xiaochen Sun, Hongzhou Zhang, Jun Xu, Qing Zhao, Rongming Wang, Dapeng Yu, Solid State Communications **129**, 803 (2004)
12. Ye Zhang, Hongbo Jia, Rongming Wang, Chinping Chen, Xuhui Luo, Dapeng Yu, Cheoljin Lee, Appl. Phys. Lett. **83**, 4631 (2003)
13. Q.X. Zhao, M. Willander, R.E. Morjan, Q.-H. Hu, E.E.B. Campbell, Appl. Phys. Lett. **83**, 165 (2003)
14. H.J. Fan, F. Fleischer, W. Lee, K. Nielsch, R. Scholz, M. Zacharias, U. Gosele, A. Dadgar, A. Krost, Superlattices and Microstructures **36**, 95 (2004)
15. Chuanbin Mao, D.J. Solis, B.D. Reiss, S.T. Kottmann, R.Y. Sweeney, A. Hayhurst, G. Georgiou, B. Iverson, A.M. Belcher, Science **303**, 213 (2004)
16. S. Banerjee, A. Dan, D. Chakravorty, J. Materials Science **37**, 4261 (2002)
17. Matt Law, Joshua Goldberger, Peidong Yang, Annu. Rev. Mater. Res. **34**, 83 (2004)
18. H. Priller, R. Hauschild, J. Zeller, C. Klingshirn, H. Kalt, R. Kling, F. Reuss, Ch. Kirchner, A. Waag, J. Lumin. **112**, 173 (2005)
19. S. Ozaki, T. Tsuchiya, Y. Inokuchi, S. Adachi, Phys. Stat. Sol. A **202**, 1325 (2005)
20. Ilan Shalish, Henryk Temkin, Venkatesh Narayanamurti, Phys. Rev. B **69**, 245401 (2004)
21. Jianfang Wang, M.S. Gudiksen, Xiangfeng Duan, Yi Cui, C.M. Lieber, Science **293**, 1455 (2001)
22. H.E. Ruda, A. Shik, Phys. Rev. B **72**, 115308 (2005)
23. C.R. McIntyre, L.J. Sham, Phys. Rev. B **45**, 9443 (1992)
24. Xin-Zheng Li, Jian-Bai Xia, Phys. Rev. B **66**, 115316 (2002)
25. S.F. Chichibu, T. Sota, G. Cantwell, E.D.B. Ason, C.W. Litton, J. Appl. Phys. **93**, 756 (2003)
26. J.B. Xia, J. Lumin. **70**, 120 (1996)
27. S. Bloom, I. Ortenburger, Phys. Stat. Sol. B **58**, 561 (1973)
28. J.R. Chelikowsky, Solid State Commun. **22**, 351 (1977)
29. M. Schlűter, J.R. Chelikowsky, S.G. Louie, M.L. Cohen, Phys. Rev. B **12**, 4200 (1975)
30. Jian-Bai Xia, K.W. Cheah, Xiao-Liang Wang, Dian-Zhao Sun, Mei-Ying Kong, Phys. Rev. B **59**, 10119 (1999)
31. Landolt-Bőrnstein, Group III, **41** B
32. A. Mang, K. Reimann, S. Rübenacke, Solid State Commun. **94**, 251 (1995)
33. Jian-Bai Xia, Jingbo Li, Phys. Rev. B **60**, 11540 (1999)
34. Jingbo Li, Jian-Bai Xia, Phys. Rev. B **62**, 12613 (2000)
35. Landolt-Bőrnstein, Group III, **17** b